Growth and thermal stability of Sc-doped BaZrO<inf>3</inf> thin films deposited on single crystal substrates

Thin Solid Films 772 (2023) 139803

Contents lists available at ScienceDirect

Thin Solid Films

journal homepage: www.elsevier.com/locate/tsf

Growth and thermal stability of Sc-doped $BaZrO_3$ thin films deposited on single crystal substrates

Gabriel K. Nzulu [a], Elena Naumovska [b], Maths Karlsson [b], Per Eklund [a], Martin Magnuson [a], Arnaud le Febvrier [a,*]

[a] Department of Physics Chemistry and Biology (IFM), Linköping University, SE-581 83 Linköping, Sweden
[b] Department of Chemistry and Chemical Engineering, Chalmers University of Technology, SE-412 96 Götheborg, Sweden

ARTICLE INFO

Keywords:
Perovskite
Temperature annealing
X-ray diffraction
Magnetron sputtering
Thin films
Oxygen deficient oxide
Proton conductor application

ABSTRACT

Thin films of $BaZr_{1-x}Sc_xO_{3-x/2}$, ($0 \leq x \leq 0.64$), well known as proton conducting solid electrolytes for intermediate temperature solid oxide fuel cell, were deposited by magnetron sputtering. X-ray diffraction analysis of the as deposited films reveals the presence of single-phase perovskite structure. The films were deposited on four different substrates (c-Al_2O_3, $LaAlO_3\langle100\rangle$, $LaAlO_3\langle110\rangle$, $LaAlO_3\langle111\rangle$) yielding random, (110)- or (100)-oriented films. The stability of the as-deposited films was assessed by annealing in air at 600 °C for 2 h. The annealing treatment revealed instabilities of the perovskite structure for the (110) and randomly oriented films, but not for (100) oriented film. The instability of the coating under heat treatment was attributed to the low oxygen content in the film (understoichiometry) prior annealing combined with the surface energy and atomic layers stacking along the growth direction. An understoichiometric (100) oriented perovskite films showed higher stability of the structure under an annealing in air at 600 °C.

1. Introduction

Acceptor-doped proton-conducting perovskite type oxides are of interest because of their potential usage as electrolytes in solid oxide fuel cells [1–4]. The perovskite ABX_3 structure, with A as large cations, B as small cations, and X an anions (O, N, F) allows substitution in either of the three sites. The substitutions of cations of different valences, compared to the host ion, yield to the possible formation of oxygen-deficient structure in which hydration of the structure can be achieved by heat treatment in a humid environment [5–7]. During this process, water molecules dissociate from the gaseous phase into hydroxyl groups (OH^-) occupying nearby oxygen vacancies site and protons (H^+) binding to the oxygen of the perovskite present initially in the perovskite. Through the process of Grotthuss type mechanism [8], protons diffuse further from the surface to the bulk by migrating from one oxygen to another in a trapping hopping mechanism. The result is an increase in material proton concentration which continues until the oxygen vacancies in the bulk are filled [8,9].

Among perovskite materials, the cubic perovskite $BaZrO_3$ shows promise for applications such as in superconductor devices [10], catalyst in transesterification [11,12], and humidity monitoring sensors [13]. Doping $BaZrO_3$ has broadened its application areas to photocatalytic water splitting process and use as electrolyte material in fuel cells [14,15]. Trivalent cation elements (Sc, Y, Gd) and other transition metals and metals elements (Co, Ni, In) are some examples of reported dopants to initiate proton conduction in $BaZrO_3$ [16–18].

When substituting a proportion of element from a perovskite the crystallographic structure may deviate from the ideal cubic perovskite structure ($Pm\bar{3}m$ space group) and yield to distinct types of disordered structures. Gold-Schmidt tolerance factor has been widely accepted as a criterion for perovskite deviation and it is measured by the mismatch between the average equilibrium A–O and B–O bond lengths. The tolerance factor can be extended to more complex perovskite when partial substitutions in the perovskite occurs such as $A_{1-x}A'_xBO_3$ or $AB_{1-x}B'_xO_3$:

$$t = \frac{(1-x)r_A + xr_{A'} + r_O}{\sqrt{2}(r_B + r_O)} \quad (1)$$

$$t = \frac{r_A + r_O}{\sqrt{2}((1-x)r_B + xr_{B'} + r_O)} \quad (2)$$

Where r_A, $r_{A'}$, r_B, $r_{B'}$ and r_O are the ionic radius of A, A', B, B' and O

* Corresponding author.
E-mail address: arnaud.le.febvrier@liu.se (A. le Febvrier).

https://doi.org/10.1016/j.tsf.2023.139803
Received 4 October 2022; Received in revised form 6 March 2023; Accepted 11 March 2023
Available online 15 March 2023

ions in the perovskite, respectively. A cubic symmetry is generally obtained for a tolerance factor in the range of $0.95 \leq t \leq 1.04$. if $t < 0.95$ or $t > 1.04$, the symmetric perovskite structure tends to reduce in a highly distorted symmetry (orthorhombic, tetragonal, trigonal structures). In the case of $BaZrO_3$, which has a nearly optimal tolerance factor of $t = 1.01$, the substitution of Zr ($r_{Zr(+IV)} = 0.720$ Å) by Sc ($r_{Sc(+III)} = 0.745$ Å) [19] gives an increase of the tolerance factor of 1.02 for $x = 0.65$ in $BaZr_{1-x}Sc_xO_{3-x/2}$. Nevertheless, the Gold-Schmidt tolerance factor has its limitation especially in the case of deficient oxygen perovskite, with the insertion of different valence elements, not considered in the calculation of the tolerance factor.

Bulk Sc-doped $BaZrO_3$ exhibited comparable to higher proton conductivity in a medium temperature range (300 – 500 °C) as yttrium-doped ceramic [9,16,20-22]. The proton conductivity is highly dependent on the content of dopants as observed for the heavily doped ones with Sc ($BaZr_{0.4}Sc_{0.6}O_3$) where the proton conductivity at 400 °C was increased to 0.012 Scm^{-1} (for comparison, Y-doped: 0.005 Scm^{-1}) [23]. More recent strategies have been proposed to further improve the proton conductivity by co-doping the different site (A, B, X) of the perovskite ABX_3 [24].

Fabrication of dense and mechanically resistance ceramic bulk of $BaZrO_3$ based material faces challenges. Generally, $BaZrO_3$ based materials ceramic require either a high sintering temperature in a range 1200–1700 °C and/or bonding material agent to improve the mechanical resistance and increase the proton mobility (ZnO, NiO, TiO_2 [18, 25-28]). The fabrication of the perovskite ceramic material in thin film form offers more favorable options in terms of control of the doping elements and the growth of dense coatings at lower temperature than the ceramic sintering. The growth of thin film on a single crystal substrate offers various possibility of preferential orientation which can be of interest for proton conductivity properties. Highly non-equilibrium deposition techniques, such as magnetron sputtering, may lead to synthesis of films with an understoichiometry nature $ABO_{3-\delta}$ [29,30]. The stoichiometry in the perovskite is primordial for the proton conduction properties of the coatings and yields to differences of the local symmetry in the material or affect the stability of the phases under heat treatment [31,32]. In contrast to the film synthesis by sputtering, the non-stoichiometry nature of the perovskite is never met in bulk synthesis where the thermodynamic equilibrium is met.

In the present study, thin film synthesis of Sc-doped $BaZrO_3$ by magnetron sputtering from an oxide $BaZrO_3$ target has been investigated. Four different single crystal substrates were used to promote the growth of different preferential orientations of the perovskite in the coating. The films were grown in a pure argon atmosphere, in a poor oxygen growth condition where the oxygen source was the oxide $BaZrO_3$ target. The effect of the insertion of Sc in $BaZr_{1-x}Sc_xO_{3-x/2}$ on the phase formation, composition, phase stability of the coatings has been studied. The different characteristics of the film dependent on their preferential orientation (different substrates) were investigated. Process control and post-annealing treatment were also investigated to understand and optimize the formation and stability perovskite $BaZr_{1-x}Sc_xO_{3-x/2}$.

2. Method and characterization

$BaZr_{1-x}Sc_xO_{3-x/2}$ thin films were deposited by magnetron sputtering on c-plane sapphire, ⟨100⟩, ⟨110⟩ and ⟨111⟩ oriented $LaAlO_3$ (LAO) substrates in an ultra-high vacuum chamber with a 3.30×10^{-07} Pa (2.5×10^{-09} Torr) base pressure at room temperature. A detailed description of the chamber can be found elsewhere [33]. Three 50 mm (2 inch) targets were used for depositing the series of samples: a $BaZrO_3$ ceramic target (from Advanced Engineering Materials Limited, 99.5%) as the main source of element; a Sc target (Plasmaterials, 99.9%) as the dopant; and a Ba target (Plasmaterials, 99.5%) to overcome any deficiency of barium. Deficiency of barium in the perovskite structure $BaZr_{1-x}Sc_xO_{3-x/2}$ may occur during deposition due to the low vapor pressure of the element and because of the doping amount where the ratio [Ba]/([Zr]+[Sc]) is aimed to be equal to 1. The 2 μm thick films were deposited on the four substrates simultaneously in equivalent position on the holder which was under a constant rotation and maintained at 600 °C. The $BaZrO_3$ target was operated at a constant rf-power of 80 W (dc equivalent bias) for all synthesized films while the Sc target was operated at dc-power between 0 and 65 W. The Ba target was operated with an rf-power between 22 W and 82 W (dc equivalent bias) to maintain the [Ba]/([Zr]+[Sc]) ratio close to 1. The detail of the deposition is listed in Table I. Prior to deposition, the substrates were cleaned with a multistep process using detergent, acetone, and ethanol in sonication bath (detergent / 5 min + 2 × distilled H_2O / 5 min, + acetone / 10 min, + ethanol / 10 min) [34]. Post deposition, the coatings were annealing at 600 °C for 2 h in air (20 °C/min), in a tubular furnace.

A Leo 1550 Gemini scanning electron microscope (SEM) equipped with an energy dispersive X-ray spectroscopy (EDS) detector operated voltage of 20 kV was used to measure their compositions and thicknesses.

The crystal structure of the films was analyzed using a PANalyical X'pert powder diffractometer in a Bragg Brentano configuration using a Cu-Kα radiation wavelength of 1.5406 Å (45 kV and 40 mA). The measurement scan was recorded with a constant rotation of the sample using a X'celerator detector in 1D scanning line mode: 10–80° 2θ range, 0.0084° step size, equivalent of 19.7 s/step.

3. Results and discussion

Table II presents the composition of the film evaluated by EDS measured on the film deposited on c-plane sapphire substrate. The composition of the films on other substrates is assumed to be the same as they were deposited at the same time in a similar holder position with constant rotation. The composition presented in table II is normalized to the perovskite "ABO_3" stoichiometry formula, considering the B site to be fully occupied (B= [Zr]+[Sc]) normalized to 1.00. The Sc content gradually increases from $x = 0$ to $x = 0.64$ in $BaZr_{1-x}Sc_xO_{3-x/2}$ when the power of the Sc target increases from 0 to 60 W. Note here that the ratio [Ba]/([Zr]+[Sc]) remained close to 1 (0.95 to 1.06) after compensating the addition of Sc and loss of Ba during the process.

Fig. 1 shows the Bragg-Brentano X-rays diffractogram of the different $BaZr_{1-x}Sc_xO_{3-x/2}$ ($0 < x < 0.64$) deposited on the four substrates. The most intense and narrower peaks observed on all the XRD patterns correspond to the substrate peaks: 006 Al_2O_3 (at $2\theta = 41.65°$) for c-Al_2O_3; 100, 200, 300 (at $2\theta = 23.46$, 47.96 and 75.11°) for LAO⟨100⟩; 110 and 220 (at $2\theta = 33.39$, 70.19°) for LAO⟨110⟩; and 111 (at $2\theta = 41.27°$) for LAO⟨111⟩ substrates. All peaks issued from the film are identified as the perovskite structure in good agreement with the $BaZrO_3$ reference ICDD data (00–006–039). Depending on the substrate, the most intense peak from $BaZrO_3$ phase differs from a randomly oriented sample revealing preferential orientations of the film. On LAO⟨111⟩, only the hhh peaks are present for a preferential orientation of the coating along the [111] direction of the perovskite structure. On the other three substrates, the most intense peaks are hh0 for c-plane sapphire and LAO⟨110⟩, and h00 for LAO⟨100⟩ substrate with a preferential orientation of the film along [110] or [100] direction, respectively.

Depending on the Sc content, other peaks with lower intensities are

Table I
Deposition parameters for all samples. $BaZrO_3$ and Ba target are powered using a Rf discharge (values as for dc equivalent) and Sc target is powered using a dc discharge.

Sample #	Deposition time (min)	$BaZrO_3$ target power (W)	Ba target Power (W)	Sc target Power (W)
1	255	80	23	0
2	235	80	45	35
3	220	80	46	25
4	205	80	60	35
5	155	80	66	60

Table II
Normalized composition of the films calculated from quantitative EDS results and normalized to the perovskite $Ba(Zr_{1-x}Sc_x)O_{3-x/2}$ with the B site of the perovskite normalized to 1.00 ([Zr] + [Sc] = 1).

Sample #	Metallic content in the perovskite ABO_3 normalized with $B = 1.00$			Sc composition (x) in $BaZr_{1-x}Sc_xO_{3-x/2}$
	Ba	Zr	Sc	
1	1.01 ± 0.05	1.00	0.00	0.00
2	0.95 ± 0.05	0.80 ± 0.04	0.20 ± 0.04	0.20
3	1.02 ± 0.04	0.64 ± 0.04	0.36 ± 0.03	0.36
4	1.05 ± 0.04	0.56 ± 0.04	0.44 ± 0.03	0.44
5	1.06 ± 0.04	0.36 ± 0.03	0.64 ± 0.03	0.64

observed corresponding to secondary orientations or a randomly orientated character of the grain. Within a substrate series and for all substrate, the addition Sc at $x = 0.2$ in the perovskite yield to a more pronounced formation of either a secondary orientation or randomly orientated character of the grain. For example, on LAO⟨110⟩ when the film has a (110) preferential orientation, the addition of Sc at $x = 0.20$ initiated the growth of (111) secondary orientation. This observation is similar on the LAO⟨100⟩and c-plane sapphire substrates. For the highest Sc content inserted ($x = 0.64$), a clear peak splitting is observed on the most intense XRD peak from $BaZrO_3$ on LAO⟨110⟩ and LAO⟨111⟩. The separation of the main diffraction peak into two peaks is not clearly distinguishable for lower Sc content and on other substrates, but differences of the XRD peak shape is noticeable for higher reflections already for Sc at x 0.36 (Fig. 1b and 1c). On LAO⟨100⟩, the XRD pattern of the (100) film with high level of Sc present one extra peak at $2\theta = 66.90°$ not initially existing in the ICDD data of $BaZrO_3$. This reflection is linked to the 300 peak with a $d = 1.396$ Å equal to $d_{100}/3$ ($2\theta = 21.20°$; $d_{100} = 4.187$ Å). This reflection is not existent for $BaZrO_3$ (JCPDS card no. 06–0399) but not forbidden by the $Pm\bar{3}m$ space group. Note that the apparition of the 300 reflection is predominant for $x \geq 0.36$ but seems to emerge already for $x = 0.20$ with a low intensity. This phenomenon is connected to a change in the structure factor due to the substitution of Sc

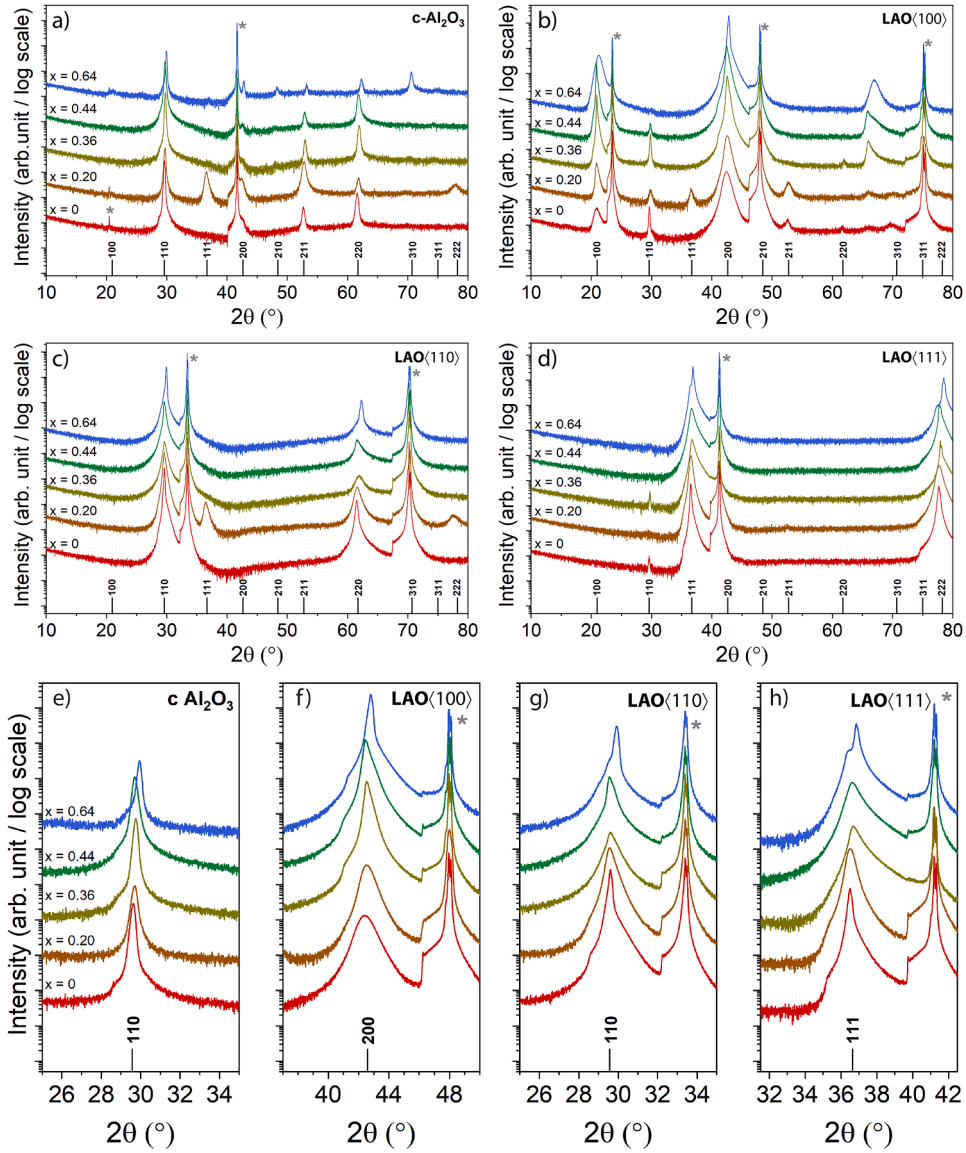

Fig. 1. XRD θ−2θ patterns of the $BaZr_{1-x}Sc_xO_{3-x/2}$ ($0 < x < 0.64$) films deposited on c-Al_2O_3 substrate, ⟨100⟩, ⟨110⟩ and ⟨111⟩ oriented $LaAlO_3$ substrates. Peaks marked with * correspond to the substrate peaks: 0006 (Al_2O_3), h00, hh0 and 111 ($LaAlO_3$). The reflection reference marks are taken from the reference bulk data for $BaZrO_3$ from JCPDS card no. 06–0399.e), f), g), h) are short range XRD pattern around the most intense peak from the coating.

in $BaZrO_3$.

Fig. 2 presents the Bragg Brentano θ−2θ patterns of the annealed $BaZr_{1-x}Sc_xO_{3-x/2}$ ($0 < x < 0.64$) films on the four substrates. The $BaZr_{1-x}Sc_xO_{3-x/2}$ film with $x = 0$ or $x = 0.20$, presents similar XRD patterns as the as-deposited sample with no changes on the shapes of the peak. Nevertheless, on c-AL_2O_3, LAO⟨110⟩ and LAO⟨111⟩, and for $x \geq 0.36$, a clear splitting of the main orientation peak appears. At higher Sc content the splitting of the peak is not clearly observed but cannot be excluded as seen by the asymmetry of the peak compared to $BaZrO_3$ reference film ($x = 0$). Within the series, split and shift of the peaks are noticeable when the Sc content increases. Note that the intensity of the two peaks observed was due to the splitting varied in intensity. For the film on LAO⟨100⟩, no splitting is observed within the series, but an increase of the full width at half maximum (FWHM) is noticeable with high Sc content.

Fig. 3 presents the evolution of the cell parameter of the as-deposited and the post-annealed coatings deposited on the four substrates in regards with the Sc content in $BaZr_{1-x}Sc_xO_{3-x/2}$ ($0 < x < 0.64$).

For the as-deposited films, on LAO⟨100⟩, the cell parameters have relatively constant values around 4.26 Å for the range $0 < x < 0.64$. On the c-plane sapphire, and LAO⟨111⟩, on addition of Sc up to $x = 0.47$ in the perovskite, the cell parameter of the perovskite remained relatively constant between 4.25 Å and 4.26 Å dependent on the substrate, and Sc content. Note here that the error bar on the evaluation of the cell parameter is larger for the film with $x = 0.37$–0.64 due to the peak shape. On LAO⟨110⟩, the cell parameters stayed constant between 4.26 Å and 4.27 Å depending on the Sc content. Except on LAO⟨100⟩, for $x = 0.64$, two cell parameter were extracted: a low cell parameter around 4.22 Å and a higher value varying between 4.27 and 4.31 Å.

After annealing at 600 °C for 2 h, two groups of sample and feature were observed. The cell parameter on the film deposited on LAO⟨100⟩ increases monotonically from 4.25 to 4.28 Å when the Sc (x) increases from 0 to 0.64 in $BaZr_{1-x}Sc_xO_{3-x/2}$. However, on the three other substrates, two cell parameters were extracted for $x \geq 0.34$ in $BaZr_{1-x}Sc_xO_{3-x/2}$: a large cell parameter following the same trend and values as the one extracted on LAO⟨100⟩, and a small cell parameter at around 4.17–4.18 Å constant for all Sc content.

In the present study, the series of films were studied to provide an

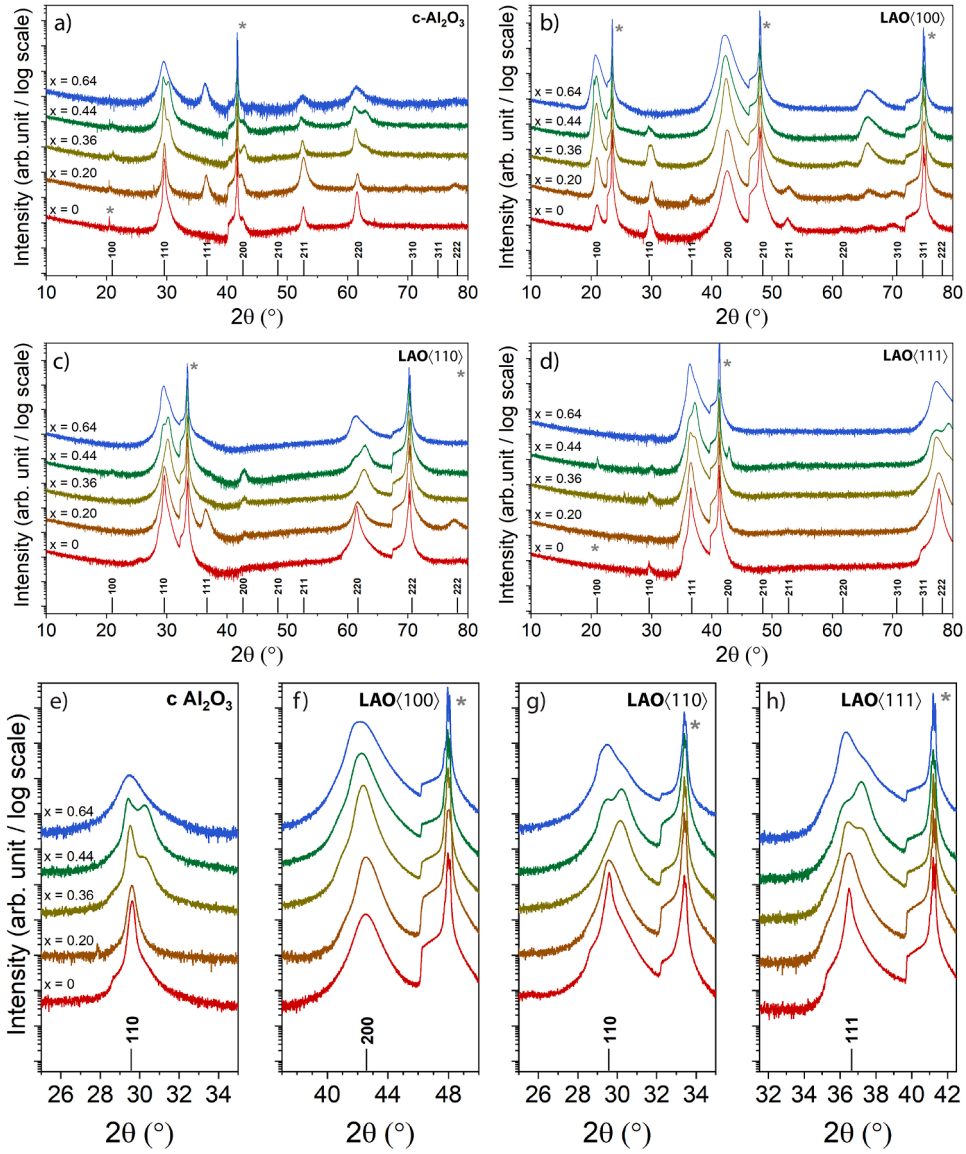

Fig. 2. XRD θ−2θ pattern of the annealed $BaZr_{1-x}Sc_xO_{3-x/2}$ ($0 < x < 0.64$) films deposited on c-Al_2O_3 substrate, ⟨100⟩, ⟨110⟩ and ⟨111⟩ oriented $LaAlO_3$ substrates. Peaks marked with * correspond to the substrate peaks: 0006 (Al_2O_3), h00, hh0 and 111 ($LaAlO_3$). The reflection reference marks are taken from the reference bulk data for $BaZrO_3$ from JCPDS card no. 06–0399. e), f), g), h) are short range XRD pattern around the most intense peak from the coating.

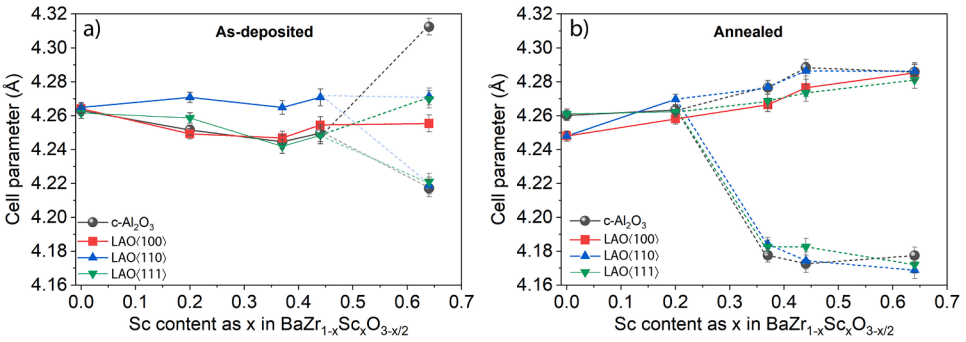

Fig. 3. Cell parameter of $BaZr_{1-x}Sc_xO_{3-x/2}$ ($0 < x < 0.64$) films deposited on the four substrates. Reported cell parameter for the a) as-deposited and b) annealed films. Cell parameter estimated from the main orientation of the film ((110) for c-Al_2O_3 and LAO⟨110⟩, (100) for LAO⟨100⟩, and (111) for LAO⟨111⟩. Note that the presence of two cell parameters for the same film/structure for the highest Sc content corresponds to the splitting/asymmetry of the peak observable on the most intense XRD peak from the film.

understanding of the formation and stability of the $BaZr_{1-x}Sc_xO_{3-x/2}$ ($0 < x < 0.64$) for possible usage as proton conductor in a fuel cell. The capability of a material to absorb H is determined after a heat treatment in a humid environment. Oxygen stoichiometry and crystallographic structure stability over a heat treatment are primordial to investigate prior possible investigation of H-absorption/conduction in $BaZr_{1-x}Sc_xO_{3-x/2}$. Therefore, the stability of the crystallographic structure of the as-deposited film was investigated after a heat treatment in air at 600 °C for 2 h.

The composition measured on the as-deposited coatings shows a stoichiometry respected within the error bars of the EDS measurement with a ratio [Ba]/([Sc]+[Zr]) close to 1 (Table II). At first glance, all films are composed of a coating with a perovskite structure isotype to the cubic $BaZrO_3$. The trends and features on the as-deposited films are challenging to discuss due to several aspects, such as thermal stress and stoichiometry in oxygen which play a role on the observations by XRD. Depending on the substrate, the growth of the perovskite occurred following specific preferential orientation (Fig. 1). From the relative intensity of the XRD peaks (cubic $BaZrO_3$ JCPDS card no. 06–0399), the coatings have a randomly oriented character on c-plane sapphire. On the contrary on LAO, preferential orientations are observed with no or few secondary orientations. LAO material, used as a substrate, is usually described with a pseudo cubic cell ($a = 3.79$ Å). For the three series on LAO substrates, the coatings follow the pseudo-cubic structure of the substrate to provide similar orientation of the perovskite on top: (100), (110) or (111).

When depositing an oxide material by magnetron sputtering, extra oxygen is usually brough as a gas to ensure the full oxidation of the coatings and allowing the formation of the right stoichiometry. In the present study, the deposition was performed in a pure Ar atmosphere, which may lead to a film with a composition in oxygen lower than expected. The deposition of understoichiometric film in oxygen by sputtering is common due to the highly thermodynamical non equilibrium process [30,35]. $BaZrO_3$ oxide target was the source of oxygen, and more metal atoms were brought by sputtering metal target (Ba and Sc). Therefore, the possibility to obtain films understoichiometric in oxygen is not excluded especially when the power of the metal target was large, thus at high Sc content. Nevertheless, in the present case, no detection of other phases (metal, fcc, bcc, hcp) than the perovskite was made using XRD, but changes in shapes of the peaks could be observed.

The splitting of the peak appearing for the highest Sc content was observed on hh0 and hhh reflections (Fig. 1, Fig. 2) revealing that the splitting is not due to a tetragonal/orthogonal deformation of the cubic perovskite but more to a segregation in to two perovskites with possibly different Sc composition. With the coatings composed of perovskite structure with lower oxygen content than expected combined with the possible thermal stress created during deposition make challenging to discuss the observation.

The heat treatment performed in air helped eliminate the oxygen vacancies and the thermal stress created during deposition. The XRD of the annealed films reveals changes in structural signature, with evidence of splitting of the peaks occurring for higher Sc content. Except for the films on LAO⟨100⟩, films on c-Al_2O_3, LAO⟨110⟩, and LAO⟨111⟩ exhibited the same feature (Figs. 2 and 3). For the coating with $x \geq 0.36$, isotype structures with two cell parameters are detected (Fig. 3). A cubic structure with a cell parameter remaining constant around 4.18 ± 0.01 Å ($0.36 < x < 0.64$) which is close to the cell parameter of bulk $BaZrO_3$ (JCPDS card no. 06–0399) [22,36]. The other perovskite phase had a cell parameter monotonically increasing from 4.26 to 4.28 Å with the Sc content ($0.36 < x < 0.64$) in a similar fashion way as the film on LAO⟨100⟩ (Fig. 3).

The investigation by XRD of the series on LAO⟨100⟩ revealed the presence of one perovskite phase for which the cell parameter varies with Sc in agreement with literature [21,37]. The possible presence of the secondary phase similar as on the other substrates is not entirely excluded as the FWHM of the diffraction peak increased for higher Sc content. Nevertheless, the peak remains symmetrical and variation of FWHM of the XRD peaks can originate from microstress, stress, crystal domains and thus makes it difficult to conclude. However, the instability phenomena observed on the coating after annealing is less pronounced or inexistent on LAO⟨100⟩.

The deposition conditions in pure argon yield to most probably to the formation of a perovskite with high oxygen vacancies. Most of the as-deposited films contain a single-phase material of $BaZr_{1-x}Sc_xO_{3-y}$ ($0 < x < 0.64$) where $y > x/2$. An annealing in air reduced the oxygen vacancies in $BaZr_{1-x}Sc_xO_{3-y}$ where $y < x/2$ and reduced the stress in the film. The heat treatment led to instabilities of the phase previously contained in the film. During annealing the films decomposed into two phases isotype to perovskite structure. This segregation may be a consequence of the relaxation of stress and oxidation process of the perovskite occurring by diffusion of the oxygen in the film through grain boundaries and within the grains. The stress relaxation and diffusion of oxygen during annealing seemed to be influenced by the film orientation. In contrast to the (111) or (110), a (100) oriented film has low surface energy of the {001} facets and provides higher stability of the surface. Unlike [001]-oriented perovskites (ABO_3) that have alternating charge neutral $A^{2+}O^{2-}/B^{4+}O_2^{4-}$layers, a [111]-oriented ABO_3 has alternating $A^{2+}O_3^{6-}/Ti^{4+}$ layers creating a stacking sequence with highly charged atomic planes. This phenomenon is enhanced by the substitution in the B site with lower valence element ($Sc^{3+} \rightarrow Zr^{4+}$). The stacking sequence yields to the rise of electric dipoles influencing the growth, driving the formation of undesired phases and undesired orientations as the material system attempts to minimize its surface energies [38,39]. Overall, the heat treatment of the high oxygen vacancy containing perovskite is detrimental for the stability of the initial phases. This phenomenon is influenced by the termination surfaces of the coatings, where instability is reduced or inhibited for a {100} terminated surfaces coating.

4. Conclusions

$BaZr_{1-x}Sc_xO_{3-x/2}$ ($0 < x < 0.64$) films were deposited on single-crystal

substrates (c-Al_2O_3, LAO⟨100⟩, LAO⟨110⟩, LAO⟨111⟩) in oxygen-deficient growth condition using magnetron sputtering. The obtained films were composed of a phase isotype as a perovskite structure where, for high Sc content ($x = 0.64$), the presence of two phases isotype as a perovskite could be observed by XRD on specific substrates. A thermal annealing in air at 600 °C for 2 h performed on the as-deposited films revealed instabilities of the perovskite structured coatings. On most of the coatings ($x \geq 0.37$), with a (110) orientation or a random orientation character of the grains, the annealing process led to the formation of two phases isotype as a perovskite structure ($BaZr_{1-x}Sc_xO_{3-x/2}$) with probably a perovskite rich in Zr and the one rich in Sc. This instability was found to be inhibited or reduced for the (100) oriented film with surface energy of the {001} facets which were grown on LAO⟨100⟩.

CRediT authorship contribution statement

Gabriel K. Nzulu: Investigation, Writing – original draft. **Elena Naumovska:** Investigation, Writing – review & editing. **Maths Karlsson:** Supervision, Writing – review & editing, Funding acquisition. **Per Eklund:** Supervision, Writing – review & editing, Funding acquisition. **Martin Magnuson:** Supervision, Writing – review & editing. **Arnaud le Febvrier:** Project administration, Conceptualization, Supervision, Writing – review & editing.

Declaration of Competing Interest

The authors declare that they have no known competing financial interests or personal relationships that could have appeared to influence the work reported in this paper.

Data availability

Data will be made available on request.

Acknowledgements

We acknowledge the Swedish Government Strategic Research Area in Materials Science on Functional Materials at Linköping University (Faculty Grant SFO-Mat-LiU No. 2009 00971), the Knut and Alice Wallenberg foundation through the Wallenberg Academy Fellows program (KAW-2020.0196), and the Swedish Energy Agency through Grant No. 48712-1 (E.N., M.K., P. E., A. l. F) and 43606-1(G.K.N., M.M.). M.M. also acknowledges financial support from the Carl Trygger Foundation (CTS20:272, CTS16:303, CTS14:310).

References

[1] H. Iwahara, T. Esaka, H. Uchida, N. Maeda, Proton conduction in sintered oxides and its application to steam electrolysis for hydrogen production, Solid State Ionics 3-4 (1981) 359–363.
[2] T. Norby, Solid-state protonic conductors: principles, properties, progress and prospects, Solid State Ionics 125 (1999) 1–11.
[3] K.D. Kreuer, Proton-Conducting Oxides, Annu. Rev. Mater. Res. 33 (2003) 333–359.
[4] N. Ito, M. Iijima, K. Kimura, S. Iguchi, New intermediate temperature fuel cell with ultra-thin proton conductor electrolyte, J. Power Sources 152 (2005) 200–203.
[5] G.P. Hammond, Energy, Environment and Sustainable Development: a UK Perspective, Process Saf. Environ. Prot. 78 (2000) 304–323.
[6] J.A. Kilner, M. Burriel, Materials for Intermediate-Temperature Solid-Oxide Fuel Cells, Annu. Rev. Mater. Res. 44 (2014) 365–393.
[7] L. Malavasi, C.A.J. Fisher, M.S. Islam, Oxide-ion and proton conducting electrolyte materials for clean energy applications: structural and mechanistic features, Chem. Soc. Rev. 39 (2010) 4370–4387.
[8] A. Fluri, E. Gilardi, M. Karlsson, V. Roddatis, M. Bettinelli, I.E. Castelli, T. Lippert, D. Pergolesi, Anisotropic Proton and Oxygen Ion Conductivity in Epitaxial Ba2In2O5 Thin Films, J. Phys. Chem. C 121 (2017) 21797–21805.
[9] L. Mazzei, M. Wolff, D. Pergolesi, J.A. Dura, L. Börjesson, P. Gutfreund, M. Bettinelli, T. Lippert, M. Karlsson, Structure and Conductivity of Epitaxial Thin Films of In-Doped $BaZrO_3$-Based Proton Conductors, J. Phys. Chem. C 120 (2016) 28415–28422.
[10] A. Erb, E. Walker, R. Flükiger, The use of $BaZrO_3$ crucibles in crystal growth of the high-Tc superconductors Progress in crystal growth as well as in sample quality, Physica C 258 (1996) 9–20.
[11] V. Singh, B.H. Hameed, Y.C. Sharma, Economically viable production of biodiesel from a rural feedstock from eastern India, P. pinnata oil using a recyclable laboratory synthesized heterogeneous catalyst, Energy Convers. Manage. 122 (2016) 52–62.
[12] Y. Yuan, X. Zhang, L. Liu, X. Jiang, J. Lv, Z. Li, Z. Zou, Synthesis and photocatalytic characterization of a new photocatalyst $BaZrO_3$, Int. J. Hydrogen Energy 33 (2008) 5941–5946.
[13] T.A. Blank, L.P. Eksperiandova, K.N. Belikov, Recent trends of ceramic humidity sensors development: a review, Sens. Actuators B 228 (2016) 416–442.
[14] L. Bi, S.P. Shafi, E. Traversa, Y-doped $BaZrO_3$ as a chemically stable electrolyte for proton-conducting solid oxide electrolysis cells (SOECs), J. Mater. Chem. A 3 (2015) 5815–5819.
[15] S. Rajendran, N.K. Thangavel, H. Ding, Y. Ding, D. Ding, L.M. Reddy Arava, Tri-Doped $BaCeO_3$–$BaZrO_3$ as a Chemically Stable Electrolyte with High Proton-Conductivity for Intermediate Temperature Solid Oxide Electrolysis Cells (SOECs), ACS Appl. Mater. Interfaces 12 (2020) 38275–38284.
[16] C.Y. Regalado Vera, H. Ding, D. Peterson, W.T. Gibbons, M. Zhou, D. Ding, A mini-review on proton conduction of $BaZrO_3$-based perovskite electrolytes, Journal of Physics: Energy 3 (2021), 032019.
[17] R. Pornprasertsuk, O. Kosasang, K. Somroop, M. Horprathum, P. Limnonthakul, P. Chindaudom, S. Jinawath, Proton conductivity of Y-doped $BaZrO_3$: pellets and thin films, Solid State Sci. 13 (2011) 1429–1437.
[18] M.K. Hossain, T. Yamamoto, K. Hashizume, Effect of sintering conditions on structural and morphological properties of Y- and Co-doped $BaZrO_3$ proton conductors, Ceram. Int. 47 (2021) 27177–27187.
[19] R.D. Shannon, Revised effective ionic radii and systematic studies of interatomic distances in halides and chalcogenides, Acta Crystallogr., Sect. A 32 (1976) 751–767.
[20] R.B. Cervera, Y. Oyama, S. Miyoshi, I. Oikawa, H. Takamura, S. Yamaguchi, Nanograined Sc-doped $BaZrO_3$ as a proton conducting solid electrolyte for intermediate temperature solid oxide fuel cells (IT-SOFCs), Solid State Ionics 264 (2014) 1–6.
[21] E. Makagon, O. Kraynis, R. Merkle, J. Maier, I. Lubomirsky, Non-Classical Electrostriction in Hydrated Acceptor Doped $BaZrO_3$: proton Trapping and Dopant Size Effect, Adv. Funct. Mater. 31 (2021), 2104188.
[22] A. Perrichon, E. Jedvik Granhed, G. Romanelli, A. Piovano, A. Lindman, P. Hyldgaard, G. Wahnström, M. Karlsson, Unraveling the Ground-State Structure of $BaZrO_3$ by Neutron Scattering Experiments and First-Principles Calculations, Chem. Mater. 32 (2020) 2824–2835.
[23] J. Hyodo, K. Kitabayashi, K. Hoshino, Y. Okuyama, Y. Yamazaki, Fast and Stable Proton Conduction in Heavily Scandium-Doped Polycrystalline Barium Zirconate at Intermediate Temperatures, Adv. Energy Mater. 10 (2020), 2000213.
[24] J. Gao, Y. Liu, Y. Meng, M. Hu, K.S. Brinkman, Fluoride-Based Anion Doping: a New Strategy for Improving the Performance of Protonic Ceramic Conductors of the Form $BaZrO_3$, ChemElectroChem 7 (2020) 2242–2247.
[25] P. Babilo, S.M. Haile, Enhanced Sintering of Yttrium-Doped Barium Zirconate by Addition of ZnO, J. Am. Ceram. Soc. 88 (2005) 2362–2368.
[26] J. Kang, G. Chen, B. Lan, R. Zhang, W. Ali, X. Lu, C. Li, Sintering behavior of Y-doped $BaZrO_3$ refractory with TiO_2 additive and effects of its dissolution on titanium melts, Int. J. Appl. Ceram. Technol. 16 (2019) 1088–1097.
[27] F.J.A. Loureiro, N. Nasani, G.S. Reddy, N.R. Munirathnam, D.P. Fagg, A review on sintering technology of proton conducting $BaCeO_3$-$BaZrO_3$ perovskite oxide materials for Protonic Ceramic Fuel Cells, J. Power Sources 438 (2019), 226991.
[28] S. Imashuku, T. Uda, Y. Awakura, Improvement in Sintering of Barium Zirconate by Doping with Scandium, ECS Trans. 7 (2007) 2321–2329.
[29] Y. Zhang, H. Sun, W. Chen, A brief review of $Ba(Ti_{0.8}Zr_{0.2})O_3$-$(Ba_{0.7}Ca_{0.3})TiO_3$ based lead-free piezoelectric ceramics: past, present and future perspectives, J. Phys. Chem. Solids 114 (2018) 207–219.
[30] R. Dittmann, 9 - Stoichiometry in epitaxial oxide thin films, in: G. Koster, M. Huijben, G. Rijnders (Eds.), Epitaxial Growth of Complex Metal Oxides, Woodhead Publishing, 2015, pp. 231–261.
[31] J. Ding, J. Balachandran, X. Sang, W. Guo, G.M. Veith, C.A. Bridges, C.M. Rouleau, J.D. Poplawsky, N. Bassiri-Gharb, P. Ganesh, R.R. Unocic, Influence of Nonstoichiometry on Proton Conductivity in Thin-Film Yttrium-Doped Barium Zirconate, ACS Appl. Mater. Interfaces 10 (2018) 4816–4823.
[32] C.A. Fuller, Q. Berrod, B. Frick, M.R. Johnson, M. Avdeev, J.S.O. Evans, I.R. Evans, Oxide Ion and Proton Conductivity in Highly Oxygen-Deficient Cubic Perovskite $SrSc_{0.3}Zn_{0.2}Ga_{0.5}O_{2.4}$, Chem. Mater. 32 (2020) 4347–4357.
[33] A. le Febvrier, L. Landälv, T. Liersch, D. Sandmark, P. Sandström, P. Eklund, An upgraded ultra-high vacuum magnetron-sputtering system for high-versatility and software-controlled deposition, Vacuum 187 (2021), 110137.
[34] A.l. Febvrier, J. Jensen, P. Eklund, Wet-cleaning of MgO(001): modification of surface chemistry and effects on thin film growth investigated by x-ray photoelectron spectroscopy and time-of-flight secondary ion mass spectroscopy, J. Vac. Sci. Technol. A 35 (2017), 021407.
[35] P. Ambwani, P. Xu, G. Haugstad, J.S. Jeong, R. Deng, K.A. Mkhoyan, B. Jalan, C. Leighton, Defects, stoichiometry, and electronic transport in SrTiO3-δ epilayers: a high pressure oxygen sputter deposition study, J. Appl. Phys. 120 (2016), 055704.
[36] S. Yamanaka, M. Fujikane, T. Hamaguchi, H. Muta, T. Oyama, T. Matsuda, S.-i. Kobayashi, K. Kurosaki, Thermophysical properties of $BaZrO_3$ and $BaCeO_3$, J. Alloys Compd. 359 (2003) 109–113.

[37] D. Kumar, B. Singh, $BaZrO_3$ and Cs-$BaZrO_3$ catalysed transesterification of Millettia Pinnata oil and optimisation of reaction variables by response surface Box-Behnken design, Renew Energy 133 (2019) 411–421.
[38] S. Schmidt, Y.-.W. Ok, D.O. Klenov, J. Lu, S.P. Keane, S. Stemmer, Microstructure of Epitaxial $SrTiO_3$/Pt/Ti/Sapphire Heterostructures, J. Mater. Res. 20 (2005) 2261–2265.
[39] S. Chakraverty, A. Ohtomo, M. Okude, K. Ueno, M. Kawasaki, Epitaxial Structure of (001)- and (111)-Oriented Perovskite Ferrate Films Grown by Pulsed-Laser Deposition, Cryst. Growth Des. 10 (2010) 1725–1729.